

Spatial kriging for replicated temporal point processes

Daniel Gervini

Department of Mathematical Sciences

University of Wisconsin–Milwaukee

July 2, 2021

Abstract

This paper presents a kriging method for spatial prediction of temporal intensity functions, for situations where a temporal point process is observed at different spatial locations. Assuming that several replications of the processes are available at the spatial sites, this method avoids assumptions like isotropy, which are not valid in many applications. As part of the derivations, new nonparametric estimators for the mean and covariance functions of temporal point processes are introduced, and their properties are studied theoretically and by simulation. The method is applied to the analysis of bike demand patterns in the Divvy bicycle sharing system of the city of Chicago.

Key words: Cox process; Poisson process; spline smoothing; tensor-product splines.

1 Introduction

In recent years, bicycle sharing systems have become increasingly common in large cities around the world (Shaheen et al., 2010). In these systems, customers can pick up and return bicycles at automated bike stations distributed within a city. Although the stations are automated, maintenance of the system requires active human management. The main issue is flow imbalance: for example, most trips during the morning commute hours tend to flow from the outer neighborhoods towards the city downtown, so neighborhood stations would quickly run out of bikes and downtown stations would quickly fill up if they were not rebalanced by trucking bikes from full stations to empty stations (Nair and Miller-Hooks, 2011). These operations, to run efficiently, require knowledge of spatio-temporal patterns of bike demand in the city. Other important aspects of system management include decisions to open, close, or relocate bike stations. To open a new bike station, the managers have to be able to forecast the patterns of bike demand at the intended new location. This is not simple, because these patterns may vary greatly within short distances (Gervini and Khanal, 2019).

From a mathematical point of view, bike demand can be modelled by spatio-temporal point processes (Gervini and Khanal, 2019). This can be done in several ways, depending on the researchers' goals. In this paper, we model bike check-out times at each station as a replicated temporal point process, where each day of the year is a replication of the process. Therefore, for a bike station located at spatial location \mathbf{s}_j , we will have n intensity functions $\{\lambda_i^j(t)\}_{i=1}^n$, one for each day. The availability of replications allows us to estimate the spatial mean and covariance of these intensity functions nonparametrically, without resorting to assumptions like isotropy which are not valid in this context (Gervini and Khanal, 2019). These estimators, in turn, can be used to predict the intensity functions $\lambda_i^0(t)$'s at a new spatial site \mathbf{s}_0 .

In the literature, the usual approach to spatial prediction is kriging (Cressie, 1993). Kriging has been extended to functional data contexts (Giraldo et al., 2010, 2011; Menafoglio et al., 2013). These methods could be applied in our context if the intensity functions at each site were estimable by smoothing, but this is not always possible because of the low daily counts at some bike stations. More importantly, these methods were developed for situations where only one observation per site is

available, which makes assumptions like isotropy unavoidable.

In this paper we present a kriging method for spatial prediction of temporal intensity functions that can be applied in anisotropic situations, when several replications of the processes are available at the spatial sites. As part of this method we introduce new nonparametric estimators for the mean and covariance functions of temporal point processes and study their properties.

2 Models and methods

2.1 Poisson point processes

A temporal point process X is a random countable set in $\mathcal{S} \subseteq (0, \infty)$ (Møller and Waagepetersen, 2004, ch. 2). The process is locally finite if $\#(X \cap B) < \infty$ with probability one for any bounded $B \subseteq \mathcal{S}$, where $\#$ denotes the cardinality of a set. In that case we define the count function $N(B) = \#(X \cap B)$ for each bounded $B \subseteq \mathcal{S}$. In particular, we define $N(t) = \#(X \cap (0, t])$. A Poisson process is a locally finite process for which there exists a locally integrable function $\lambda : \mathcal{S} \rightarrow [0, \infty)$, called the intensity function, such that (i) $N(B)$ has a Poisson distribution with rate $\int_B \lambda(t) dt$, and (ii) for disjoint sets B_1, \dots, B_k in \mathcal{S} the random variables $N(B_1), \dots, N(B_k)$ are independent. A consequence of (i) and (ii) is that the conditional distribution of the points in $X \cap B$ given $N(B) = m$ is the distribution of m independent and identically distributed observations with density $\lambda(t) / \int_B \lambda$. In this paper we will mostly consider temporal processes defined on a common bounded interval $\mathcal{S} = [a, b]$, for example $\mathcal{S} = [0, 24]$ for daily processes.

For replicated point processes, a single intensity function λ rarely provides an adequate fit for all replications; it is more reasonable to assume that λ itself is the realization of a random process Λ and thus changes from replication to replication. Such compound processes are called doubly stochastic or Cox processes (Møller and Waagepetersen, 2004, ch. 5). A doubly stochastic Poisson process is a pair (X, Λ) where $X|\Lambda = \lambda$ is a Poisson process with intensity function λ , and Λ is a random function that takes values on the space \mathcal{F} of non-negative locally integrable functions on \mathcal{S} . Thus the n daily replications of the process can be modeled as n independent and identically distributed pairs $(X_1, \Lambda_1), \dots, (X_n, \Lambda_n)$. The latent process Λ is not directly observable; only X is observed.

In our applications we observe temporal processes at d different spatial locations. This can be modeled as a multivariate doubly stochastic process $(\mathbf{X}, \mathbf{\Lambda})$ with $\mathbf{X} = (X^1, \dots, X^d)$ and $\mathbf{\Lambda} = (\Lambda^1, \dots, \Lambda^d)$, where the X^j s are conditionally independent given $\mathbf{\Lambda} = \boldsymbol{\lambda}$. The dependencies among the X^j s are then determined by the dependencies among the Λ^j s. Since each Λ^j is associated with a specific spatial location \mathbf{s}_j , we will make this explicit in the notation by writing $\Lambda^j(t) = \Lambda(t, \mathbf{s}_j)$, but $\Lambda(t, \mathbf{s})$ is not a joint spatio-temporal intensity function, it is only a temporal intensity function in t for each \mathbf{s} .

2.2 Spatial kriging

The unbiased kriging predictor of $\Lambda(t, \mathbf{s}_0)$, the intensity process at a new spatial location \mathbf{s}_0 , based on $\Lambda(t, \mathbf{s}_1), \dots, \Lambda(t, \mathbf{s}_d)$ is

$$\Lambda^*(t, \mathbf{s}_0) = \sum_{j=1}^d c_j^* \Lambda(t, \mathbf{s}_j),$$

where $\mathbf{c}^* = (c_1^*, \dots, c_d^*)$ minimizes the squared prediction error

$$\text{SPE}(\mathbf{c}) = E\left\{\left\|\Lambda(\cdot, \mathbf{s}_0) - \sum_{j=1}^d c_j \Lambda(\cdot, \mathbf{s}_j)\right\|^2\right\} \quad (1)$$

subject to the unbiasedness constraint

$$\mu(t, \mathbf{s}_0) = \sum_{j=1}^d c_j \mu(t, \mathbf{s}_j), \quad (2)$$

where $\mu(t, \mathbf{s}) = E\{\Lambda(t, \mathbf{s})\}$ and $\|\cdot\|$ is the L_2 norm.

The squared prediction error (1), in view of the constraints (2), comes down to

$$\text{SPE}(\mathbf{c}) = \mathbf{c}^T \boldsymbol{\Sigma} \mathbf{c} - 2\mathbf{c}^T \boldsymbol{\sigma}_0 + \sigma_{00}, \quad (3)$$

where $\boldsymbol{\Sigma}$ has elements

$$\Sigma_{jk} = \int \text{cov}\{\Lambda(t, \mathbf{s}_j), \Lambda(t, \mathbf{s}_k)\} dt, \quad (4)$$

$\boldsymbol{\sigma}_0$ has elements

$$\sigma_{0j} = \int \text{cov} \{ \Lambda(t, \mathbf{s}_j), \Lambda(t, \mathbf{s}_0) \} dt, \quad (5)$$

and $\sigma_{00} = \int \text{var} \{ \Lambda(t, \mathbf{s}_0) \} dt$. By multiplying both sides of (2) by the $\mu(t, \mathbf{s}_k)$'s and integrating t out, the constraints can be expressed as

$$\mathbf{M}\mathbf{c} = \mathbf{m}_0, \quad (6)$$

where \mathbf{M} has elements

$$M_{jk} = \int \mu(t, \mathbf{s}_j) \mu(t, \mathbf{s}_k) dt \quad (7)$$

and \mathbf{m}_0 has elements

$$m_{0j} = \int \mu(t, \mathbf{s}_j) \mu(t, \mathbf{s}_0) dt. \quad (8)$$

When \mathbf{M} is full rank, the minimization of (3) subject to (6) has a closed-form solution

$$\begin{bmatrix} \mathbf{c}^* \\ \ell \end{bmatrix} = \begin{bmatrix} \boldsymbol{\Sigma} & \mathbf{M}^T \\ \mathbf{M} & \mathbf{O} \end{bmatrix}^{-1} \begin{bmatrix} \boldsymbol{\sigma}_0 \\ \mathbf{m}_0 \end{bmatrix},$$

where $\ell \in \mathbb{R}^d$ is the Lagrange multiplier and \mathbf{O} is the $d \times d$ zero matrix. To compute \mathbf{c}^* , then, it is necessary to obtain estimators of $\boldsymbol{\Sigma}$, $\boldsymbol{\sigma}_0$, \mathbf{M} , and \mathbf{m}_0 , which will be introduced in Section 2.3.

The $d \times d$ matrix \mathbf{M} is often not full rank. For example, if $\mu(t, \mathbf{s}_j) \equiv \mu(t)$ for all \mathbf{s}_j , then \mathbf{M} has rank one. Even when it has full rank, \mathbf{M} is often ill-conditioned, with many eigenvalues near zero. In those situations \mathbf{M} can be truncated as follows. Let $\mathbf{M} = \mathbf{U}\boldsymbol{\Delta}\mathbf{U}^T$ be the spectral decomposition of \mathbf{M} , where $\boldsymbol{\Delta} = \text{diag}(\delta_1, \dots, \delta_d)$ are the eigenvalues of \mathbf{M} in decreasing order and \mathbf{U} is an orthogonal matrix of eigenvectors. Let r be the number of δ_j 's that are strictly positive; or, in practice, we can take the smallest r such that $\sum_{j=1}^r \delta_j / \sum_{j=1}^d \delta_j \geq 0.9$, say. Then the d -dimensional constraints (6) are replaced by the r -dimensional approximation

$$\tilde{\mathbf{M}}\mathbf{c} = \tilde{\mathbf{m}}_0, \quad (9)$$

where $\tilde{\mathbf{M}} = \boldsymbol{\Delta}_r \mathbf{U}_r^T$, $\tilde{\mathbf{m}}_0 = \mathbf{U}_r^T \mathbf{m}_0$, $\boldsymbol{\Delta}_r = \text{diag}(\delta_1, \dots, \delta_r)$, and \mathbf{U}_r are the first r columns of \mathbf{U} .

We note that although the kriging prediction problem was framed in terms of the

unobservable intensity processes $\Lambda^j(t)$'s, the estimated kriging coefficients $\hat{\mathbf{c}}^*$, once obtained, can also be used for direct real-time prediction of the count functions: for a given day i , the predicted count function at the new site \mathbf{s}_0 would be $N_i^{0*}(t) = \sum_{j=1}^d c_j^* N_i^j(t)$, where the $N_i^j(t)$'s are the observed count functions at the sites \mathbf{s}_j 's. This is an unbiased predictor, in view of (2), since $E\{N^0(t)\} = \int_a^t \mu(t, \mathbf{s}_0) dt$ and $E\{N^j(t)\} = \int_a^t \mu(t, \mathbf{s}_j) dt$.

2.3 Mean and covariance estimation

2.3.1 Nonparametric estimators at observed sites

Estimation of the mean functions $\mu_j(t) = \mu(t, \mathbf{s}_j)$ and the covariance functions $\rho_{jk}(t, t') = \text{cov}\{\Lambda(t, \mathbf{s}_j), \Lambda(t', \mathbf{s}_k)\}$ at the spatial points \mathbf{s}_j and \mathbf{s}_k where data is available can be done as follows. Since $X^j \mid \Lambda^j = \lambda^j$ is a Poisson process with intensity function $\lambda^j(t)$, for any integrable functions $f(t)$ and $g(t)$ we have, as shown in the Supplementary Material,

$$E\left\{\sum_{t \in X^j} f(t)\right\} = \int f(t) \mu_j(t) dt, \quad (10)$$

$$E\left\{\sum_{t \in X^j} \sum_{t' \in X^k} f(t)g(t')\right\} = \iint f(t)g(t') R_{jk}(t, t') dt dt', \text{ for } j \neq k, \quad (11)$$

and

$$E\left\{\sum_{t \in X^j} \sum_{t' \in X^j, t' \neq t} f(t)g(t')\right\} = \iint f(t)g(t') R_{jj}(t, t') dt dt', \quad (12)$$

where $R_{jk}(t, t') = E\{\Lambda(t, \mathbf{s}_j)\Lambda(t', \mathbf{s}_k)\}$. Now consider a B -spline basis (De Boor, 2001, ch. 9) $\boldsymbol{\beta}(t) = (\beta_1(t), \dots, \beta_p(t))^T$ on $[a, b]$, and let $\mathbf{G} = \int \boldsymbol{\beta}(t)\boldsymbol{\beta}(t)^T dt$. Then, given independent and identically distributed replications $\mathbf{X}_1, \dots, \mathbf{X}_n$ of the multivariate process \mathbf{X} , define

$$\hat{\mu}_j(t) = \boldsymbol{\beta}(t)^T \mathbf{G}^{-1} \frac{1}{n} \sum_{i=1}^n \sum_{u \in X_i^j} \boldsymbol{\beta}(u), \quad (13)$$

$$\hat{R}_{jk}(t, t') = \boldsymbol{\beta}(t)^T \mathbf{G}^{-1} \left\{ \frac{1}{n} \sum_{i=1}^n \sum_{u \in X_i^j} \sum_{v \in X_i^k} \boldsymbol{\beta}(u) \boldsymbol{\beta}(v)^T \right\} \mathbf{G}^{-1} \boldsymbol{\beta}(t'), \text{ for } j \neq k, \quad (14)$$

and

$$\hat{R}_{jj}(t, t') = \boldsymbol{\beta}(t)^T \mathbf{G}^{-1} \left\{ \frac{1}{n} \sum_{i=1}^n \sum_{u \in X_i^j} \sum_{v \in X_i^j, v \neq u} \boldsymbol{\beta}(u) \boldsymbol{\beta}(v)^T \right\} \mathbf{G}^{-1} \boldsymbol{\beta}(t'). \quad (15)$$

The consistency of these estimators as the number of replications n goes to infinity is proved in Section 3, and confirmed by simulations in Section 4.

From the above $\hat{\mu}_j(t)$'s and $\hat{R}_{jk}(t, t')$'s we obtain $\hat{\rho}_{jk}(t, t') = \hat{R}_{jk}(t, t') - \hat{\mu}_j(t) \hat{\mu}_k(t')$. These are plugged into equations (7) to obtain $\hat{\mathbf{M}}$ and (4) to obtain $\hat{\boldsymbol{\Sigma}}$.

It is often the case that $\hat{\boldsymbol{\Sigma}}$, although full rank, is ill-conditioned. We found out in our simulation studies that truncating $\hat{\boldsymbol{\Sigma}}$ improves kriging accuracy. As before, let $\hat{\boldsymbol{\Sigma}} = \mathbf{V} \mathbf{H} \mathbf{V}^T$ be the spectral decomposition of $\hat{\boldsymbol{\Sigma}}$, where $\mathbf{H} = \text{diag}(\eta_1, \dots, \eta_d)$ are the eigenvalues of $\hat{\boldsymbol{\Sigma}}$ in decreasing order and \mathbf{V} is an orthogonal matrix of eigenvectors. Take the smallest s such that $\sum_{j=1}^s \eta_j / \sum_{j=1}^d \eta_j \geq 0.9$. Let $\mathbf{H}_s = \text{diag}(\eta_1, \dots, \eta_s)$ and let \mathbf{V}_s be the first s columns of \mathbf{V} . Then solve

$$\begin{bmatrix} \hat{\mathbf{c}}_s \\ \hat{\ell} \end{bmatrix} = \begin{bmatrix} \mathbf{H}_s & \mathbf{V}_s^T \hat{\mathbf{M}}^T \\ \hat{\mathbf{M}} \mathbf{V}_s & \mathbf{O} \end{bmatrix}^{-1} \begin{bmatrix} \mathbf{V}_s^T \hat{\boldsymbol{\sigma}}_0 \\ \hat{\mathbf{m}}_0 \end{bmatrix}$$

and take $\hat{\mathbf{c}}^* = \mathbf{V}_s \hat{\mathbf{c}}_s$. Of course, if $\hat{\mathbf{M}}$ and $\hat{\mathbf{m}}_0$ are truncated as in (9), then their truncated versions should be used instead.

2.3.2 Estimators at the new site

To estimate $\boldsymbol{\sigma}_0$ and \mathbf{m}_0 , the above mean and covariance estimators are extended by smoothing to spatial points \mathbf{s}_0 where no data is available. Consider first the mean function $\mu(t, \mathbf{s})$. We model this function as $\boldsymbol{\beta}(t)^T \mathbf{B} \boldsymbol{\gamma}(\mathbf{s})$, where $\boldsymbol{\gamma}(\mathbf{s}) = (\gamma_1(\mathbf{s}), \dots, \gamma_q(\mathbf{s}))^T$ is a spatial basis on R , a region of \mathbb{R}^2 that includes \mathbf{s}_0 and the \mathbf{s}_k 's, and \mathbf{B} is a matrix of coefficients to be estimated from the data. In this paper we use tensor-product splines as $\boldsymbol{\gamma}(\mathbf{s})$ (De Boor, 2001, ch. 17), but other alternatives are possible, like thin-plate splines (Wahba, 1990) or radial basis functions (Buhmann, 2003).

To estimate \mathbf{B} , note that $\hat{\mu}_j(t)$ in (13) has the form $\hat{\mu}_j(t) = \boldsymbol{\beta}(t)^T \hat{\mathbf{a}}_j$, with

$$\hat{\mathbf{a}}_j = \mathbf{G}^{-1} \frac{1}{n} \sum_{i=1}^n \sum_{u \in X_i^j} \boldsymbol{\beta}(u),$$

so the penalized least squares estimator of \mathbf{B} is

$$\hat{\mathbf{B}} = \arg \min_{\mathbf{B}} \sum_{j=1}^d \|\hat{\mathbf{a}}_j - \mathbf{B}\boldsymbol{\gamma}(\mathbf{s}_j)\|^2 + \xi_B P_1(\mathbf{B}),$$

where $P_1(\mathbf{B})$ is a roughness penalty function and ξ_B a smoothing parameter. As explained in the Supplementary Material, if the roughness of a bivariate function $f(s^1, s^2)$ is measured by $\iint (\sum_{1 \leq i, j \leq 2} f_{ij}^2) ds^1 ds^2$, where $f_{ij} = \partial^2 f / \partial s^i \partial s^j$, then $P_1(\mathbf{B}) = \text{tr}(\mathbf{B}^T \mathbf{B} \mathbf{J})$, where \mathbf{J} is a matrix that depends only on $\boldsymbol{\gamma}(\mathbf{s})$, and the closed form of $\hat{\mathbf{B}}$ is

$$\hat{\mathbf{B}} = \mathbf{A} \boldsymbol{\Gamma} (\boldsymbol{\Gamma}^T \boldsymbol{\Gamma} + \xi_B \mathbf{J})^{-1}, \quad (16)$$

where $\boldsymbol{\Gamma} = [\boldsymbol{\gamma}(\mathbf{s}_1), \dots, \boldsymbol{\gamma}(\mathbf{s}_d)]^T$ and $\mathbf{A} = [\hat{\mathbf{a}}_1, \dots, \hat{\mathbf{a}}_d]$. Once $\hat{\mathbf{B}}$ is obtained, $\mu(t, \mathbf{s}_0)$ is estimated by $\hat{\mu}(t, \mathbf{s}_0) = \boldsymbol{\beta}(t)^T \hat{\mathbf{B}} \boldsymbol{\gamma}(\mathbf{s}_0)$ and plugged into (8) to obtain $\hat{\mathbf{m}}_0$.

The optimal smoothing parameter ξ_B can be chosen by cross-validation (Hastie et al., 2009, ch. 7). The leave-one-site-out cross-validation statistic would be

$$\begin{aligned} \text{CV}(\xi_B) &= \frac{1}{d} \sum_{j=1}^d \|\hat{\mathbf{a}}_j - \hat{\mathbf{B}}_{(j)} \boldsymbol{\gamma}(\mathbf{s}_j)\|^2 \\ &= \frac{1}{d} \sum_{j=1}^d \frac{\|\hat{\mathbf{a}}_j - \hat{\mathbf{B}} \boldsymbol{\gamma}(\mathbf{s}_j)\|^2}{(1 - h_{B,jj})^2}, \end{aligned}$$

where $\hat{\mathbf{B}}_{(j)}$ is the \mathbf{s}_j -deleted version of $\hat{\mathbf{B}}$, and $h_{B,jj}$ is the j th diagonal element of the hat matrix $\mathbf{H}_B = \boldsymbol{\Gamma} (\boldsymbol{\Gamma}^T \boldsymbol{\Gamma} + \xi_B \mathbf{J})^{-1} \boldsymbol{\Gamma}^T$. If $\text{df}_B = \text{tr}(\mathbf{H}_B)$ are the degrees of freedom, then $h_{B,jj} \approx \text{df}_B / d$ and the generalized cross-validation statistic is

$$\text{GCV}(\xi_B) = \frac{1}{d} \sum_{j=1}^d \frac{\|\hat{\mathbf{a}}_j - \hat{\mathbf{B}} \boldsymbol{\gamma}(\mathbf{s}_j)\|^2}{(1 - \text{df}_B / d)^2}.$$

The optimal $\hat{\xi}_B$ is chosen as the minimizer of $\text{GCV}(\xi_B)$.

To estimate $\boldsymbol{\sigma}_0$ we also use spatial smoothing and model $\Sigma(\mathbf{s}, \mathbf{s}') = \int \text{cov} \{ \Lambda(t, \mathbf{s}), \Lambda(t, \mathbf{s}') \} dt$

by $\gamma(\mathbf{s})^T \mathbf{C} \gamma(\mathbf{s}')$, with \mathbf{C} symmetric. The penalized least squares estimator of \mathbf{C} is

$$\hat{\mathbf{C}} = \arg \min_{\mathbf{C}} \sum_{j=1}^d \sum_{\substack{k=1 \\ k \neq j}}^d \left\{ \hat{\Sigma}_{jk} - \gamma(\mathbf{s}_j)^T \mathbf{C} \gamma(\mathbf{s}_k) \right\}^2 + \xi_C P_2(\mathbf{C}), \quad (17)$$

where, as before, $P_2(\mathbf{C})$ is a roughness penalty function and ξ_C is a smoothing parameter. Here we use only the off-diagonal elements $\hat{\Sigma}_{jk}$ with $j \neq k$ for estimation, because, in most applications, the intrinsic variability at each spatial site creates a ridge that makes $\Sigma(\mathbf{s}, \mathbf{s}')$ discontinuous at the diagonal $\mathbf{s} = \mathbf{s}'$.

If the roughness of a function $f(s^1, s^2, s^3, s^4)$ is measured by $\iint (\sum_{1 \leq i,j,k,l \leq 2} f_{ijkl}^2) ds^1 ds^2 ds^3 ds^4$, then $P_2(\mathbf{C}) = \text{tr}\{(\mathbf{C}\mathbf{J})^2\}$ with the same \mathbf{J} as before. As shown in the Supplementary Material, the closed form for $\text{vec}(\hat{\mathbf{C}})$ is

$$\text{vec}(\hat{\mathbf{C}}) = \mathbf{\Omega}^{-1}(\mathbf{\Gamma}^T \otimes \mathbf{\Gamma}^T) \text{vec}(\hat{\mathbf{\Sigma}} - \text{diag } \hat{\mathbf{\Sigma}}), \quad (18)$$

where $\mathbf{\Omega} = \{(\mathbf{\Gamma}^T \otimes \mathbf{\Gamma}^T)(\mathbf{I} - \mathbf{E}^T \mathbf{E})(\mathbf{\Gamma} \otimes \mathbf{\Gamma}) + \xi_C(\mathbf{J} \otimes \mathbf{J})\}$, $\mathbf{E}^T \mathbf{E} = \sum_{j=1}^d \mathbf{e}_j \mathbf{e}_j^T \otimes \mathbf{e}_j \mathbf{e}_j^T$ and \mathbf{e}_j is the j -th canonical vector in \mathbb{R}^d . Once $\hat{\mathbf{C}}$ has been obtained, the σ_{0j} 's in (5) are estimated by $\hat{\sigma}_{0j} = \gamma(\mathbf{s}_j)^T \hat{\mathbf{C}} \gamma(\mathbf{s}_0)$. Details of numerical implementation are also discussed in the Supplementary Material, since the large dimension of $\mathbf{\Omega}$ would make straightforward implementation of (18) very inefficient and time consuming.

The optimal smoothing parameter ξ_C can be found, as before, by generalized cross-validation. The leave-one- (j, k) -out cross-validation statistic is

$$\begin{aligned} \text{CV}(\xi_C) &= \frac{1}{d(d-1)} \sum_{j=1}^d \sum_{\substack{k=1 \\ k \neq j}}^d \left\{ \hat{\Sigma}_{jk} - \gamma(\mathbf{s}_j)^T \hat{\mathbf{C}}_{(j,k)} \gamma(\mathbf{s}_k) \right\}^2 \\ &= \frac{1}{d(d-1)} \sum_{j=1}^d \sum_{\substack{k=1 \\ k \neq j}}^d \frac{\left\{ \hat{\Sigma}_{jk} - \gamma(\mathbf{s}_j)^T \hat{\mathbf{C}} \gamma(\mathbf{s}_k) \right\}^2}{(1 - h_{C,(j,k)})^2}, \end{aligned}$$

where $\hat{\mathbf{C}}_{(j,k)}$ is the (j, k) -deleted version of $\hat{\mathbf{C}}$ and $h_{C,(j,k)}$ is the diagonal element of the hat matrix $\mathbf{H}_C = (\mathbf{\Gamma} \otimes \mathbf{\Gamma}) \mathbf{\Omega}^{-1} (\mathbf{\Gamma}^T \otimes \mathbf{\Gamma}^T)$ corresponding to the location of $\hat{\Sigma}_{jk}$ in $\text{vec}(\hat{\mathbf{\Sigma}})$. If $\text{df}_C = \text{tr}(\mathbf{H}_C)$, then $h_{C,(j,k)} \approx \text{df}_C / d(d-1)$ and the generalized

cross-validation statistic is

$$\text{GCV}(\xi_C) = \frac{1}{d(d-1)} \sum_{j=1}^d \sum_{\substack{k=1 \\ k \neq j}}^d \frac{\left\{ \hat{\Sigma}_{jk} - \gamma(\mathbf{s}_j)^T \hat{\mathbf{C}} \gamma(\mathbf{s}_k) \right\}^2}{\{1 - \text{df}_C/d(d-1)\}^2}.$$

The optimal $\hat{\xi}_C$ is chosen as the minimizer of $\text{GCV}(\xi_C)$.

3 Asymptotics

In this section we establish the consistency of the nonparametric estimators of the mean and covariance functions introduced in Section 2.3.1. The convergence rates that we obtain are in line with the standard asymptotic results for regression splines (Agarwal and Studden, 1980; Zhou et al., 1998).

We assume that the B -spline basis $\beta(t)$ has order r and is defined by a knot sequence $\{\tau_1, \dots, \tau_k\}$ that is regular, in the sense that

$$\int_a^{\tau_i} g(t) dt = \frac{i}{k+1}, \quad i = 1, \dots, k,$$

for a strictly positive density function $g(t)$ on $[a, b]$. The basis dimension p is then $r + k$. The observed point processes $\mathbf{X}_1, \dots, \mathbf{X}_n$ are assumed to be independent and identically distributed replications of a d -variate doubly stochastic Poisson process \mathbf{X} with latent intensity process $\mathbf{\Lambda}$, as explained in Section 2.1. The norm $\|\cdot\|$ below is the standard $L_2[a, b]$ norm, and $L_2^r[a, b]$ is the Sobolev space of functions f such that $D^{r-1}f$ is absolutely continuous on $[a, b]$ and $D^r f \in L_2[a, b]$, where D denotes differentiation. Proofs of the results in this section are given in the Supplementary Material.

Theorem 1 *Let $\hat{\mu}_j(t)$ be the estimator defined in (13), and suppose that $\mu_j \in L_2^r[a, b]$. Then*

$$E\|\hat{\mu}_j - \mu_j\|^2 = \frac{1}{n}O(k) + O\left(\frac{1}{k^{2r}}\right).$$

The fastest convergence rate is attained for $k = O(n^{1/(2r+1)})$, in which case $E\|\hat{\mu}_j - \mu_j\|^2 = O(n^{-2r/(2r+1)})$.

Theorem 1 shows that the optimal nonparametric convergence rate $O(n^{-2r/(2r+1)})$

for functions in $L_2^r[a, b]$ (Stone, 1982) is attained by $\hat{\mu}_j(t)$ if k is chosen appropriately. For cubic splines, $r = 4$ and then the optimal rates are $k = O(n^{1/9})$ and $E\|\hat{\mu}_j - \mu_j\|^2 = O(n^{-8/9})$. The number of knots k , then, should grow slowly with n , since, for example, $400^{1/9} \approx 2$.

The next theorem gives convergence rates for the $\hat{R}_{jk}(t, t')$'s. Now $\|\cdot\|$ is the $L_2([a, b] \times [a, b])$ norm and $L_2^{(r,r)}([a, b] \times [a, b])$ is the tensor Sobolev space of bivariate functions f such that $D_i^{r-1}f$ is absolutely continuous on $[a, b] \times [a, b]$ and $D_i^r f \in L_2([a, b] \times [a, b])$, where D_i denotes differentiation with respect to the i -th variable.

Theorem 2 *Let $\hat{R}_{jk}(t, t')$ be the estimator defined in (14), if $j \neq k$, or in (15), if $j = k$. Then, if $R_{jk} \in L_2^{(r,r)}([a, b] \times [a, b])$, we have*

$$E\|\hat{R}_{jk} - R_{jk}\|^2 = \frac{1}{n}O(k^2) + O\left(\frac{1}{k^{2r}}\right).$$

The fastest convergence rate is attained for $k = O(n^{1/(2r+2)})$, in which case $E\|\hat{R}_{jk} - R_{jk}\|^2 = O(n^{-2r/(2r+2)})$.

Once again, Theorem 2 shows that the optimal convergence rate $O(n^{-2r/(2r+2)})$ for bivariate functions (Stone, 1994) is attained by $\hat{R}_{jk}(t, t')$ if k is suitably chosen. For cubic splines, the optimal k would have rate $O(n^{1/10})$ and the squared estimation error would have rate $O(n^{-8/10})$. According to Theorems 1 and 2, the optimal rates for k are different for the $\hat{\mu}_j(t)$'s and the $\hat{R}_{jk}(t, t')$'s. However, for simplicity we use the same spline basis $\beta(t)$ in all cases.

4 Simulations

In this section we study by simulation the consistency and convergence rates of the mean and covariance estimators introduced in Sections 2.3.1 and 2.3.2, and of the kriging predictors introduced in Section 2.2. We are specifically interested in the effects of sample size n , spatial grid size d , and grid spacing $\delta = \min_{j \neq k} \|\mathbf{s}_j - \mathbf{s}_k\|$ on estimation and prediction error.

To this end we simulated the following scenarios. Three spatial grids were considered: (i) $d = 16$ uniformly spaced \mathbf{s}_j 's on the square $[-0.5, 0.5] \times [-0.5, 0.5]$, (ii) $d = 16$ uniformly spaced \mathbf{s}_j 's on the square $[-0.2, 0.2] \times [-0.2, 0.2]$, and (iii) $d = 64$

uniformly spaced \mathbf{s}_j 's on the square $[-0.5, 0.5] \times [-0.5, 0.5]$. The respective grid spacings are (i) $\delta = 0.33$, (ii) $\delta = 0.13$, and (iii) $\delta = 0.14$. Grids (i) and (iii) cover the same range but a larger d makes (iii) denser, while grids (i) and (ii) have the same size d but (ii) is denser because it covers a smaller range. The kriging predictor was evaluated at the spatial point $\mathbf{s}_0 = (0, 0)$.

The latent processes $\Lambda(t, \mathbf{s}_j)$'s were generated according to the log-Gaussian model

$$\Lambda(t, \mathbf{s}_j) = \exp\{\nu(t) + U_j\phi(t)\} \quad (19)$$

for $t \in [0, 1]$, with $\nu(t) = \sin(\pi t) + \ln 20$ and $\phi(t) = \sqrt{2}\sin(\pi t)$. The U_j 's, which determine the spatial correlations, were defined as

$$U_j = g(\mathbf{s}_j)W + E_j \quad (20)$$

with $W \sim N(0, 0.072)$ and $E_j \sim N(0, 0.018)$. The E_j 's were independent among themselves and of W . Two functions $g(\mathbf{s})$ were considered: Model 1, $g(\mathbf{s}) = 1/(1 + \|\mathbf{s}\|)$, and Model 2, $g(\mathbf{s}) = 1$. The common factor $g(\mathbf{s})W$ in (20) makes $\text{cov}\{\Lambda(t, \mathbf{s}), \Lambda(t, \mathbf{s}')\}$ a smooth function for $\mathbf{s} \neq \mathbf{s}'$, but the E_j 's create a ridge at $\mathbf{s} = \mathbf{s}'$, as noted in Section 2.3.2. Explicit expressions for $\mu(t, \mathbf{s}_j)$ and $\text{cov}\{\Lambda(t, \mathbf{s}_j), \Lambda(t, \mathbf{s}_k)\}$ are given in the Supplementary Material.

For estimation we used cubic B -splines with five equally-spaced knots as temporal basis $\beta(t)$, and tensor-product cubic B -splines with six equally-spaced knots on each coordinate as spatial basis $\gamma(\mathbf{s})$. The respective basis dimensions are $p = 9$ and $q = 100$. The optimal smoothing parameters ξ_B and ξ_C were chosen by generalized cross-validation, as explained in Section 2.3. Four sample sizes n were considered: 50, 100, 200, and 400. Each scenario was replicated 400 times.

We are mainly interested in estimation of the quantities \mathbf{M} and \mathbf{m}_0 in (6), of Σ in (4), and of σ_0 in (5), because they are needed for kriging. For $\hat{\mathbf{M}}$ we define the relative error measures: $\text{bias}(\hat{\mathbf{M}}) = \|E \text{vech } \hat{\mathbf{M}} - \text{vech } \mathbf{M}\| / \|\text{vech } \mathbf{M}\|$, $\text{sd}(\hat{\mathbf{M}}) = \{E \|\text{vech } \hat{\mathbf{M}} - E \text{vech } \hat{\mathbf{M}}\|^2\}^{1/2} / \|\text{vech } \mathbf{M}\|$, and $\text{rmse}(\hat{\mathbf{M}}) = \{E \|\text{vech } \hat{\mathbf{M}} - \text{vech } \mathbf{M}\|^2\}^{1/2} / \|\text{vech } \mathbf{M}\|$, where vech denotes the vectorization of the lower triangular part of a matrix and $\|\cdot\|$ the usual Euclidean norm. Analogous measures are defined for $\hat{\mathbf{m}}_0$, $\text{vech } \hat{\Sigma}$, and $\hat{\sigma}_0$. To assess the accuracy of the kriging predictor we compared the best SPE (1) attained by the true parameters, SPE_0 , with the SPE attained by the estimators, $\widehat{\text{SPE}}$. Since $\widehat{\text{SPE}} \geq \text{SPE}_0$, $\text{bias}(\widehat{\text{SPE}}) = \text{rmse}(\widehat{\text{SPE}})$. The rmse's for all parameters are reported in

Grid	n	Model 1					Model 2				
		\mathbf{M}	\mathbf{m}_0	$\mathbf{\Sigma}$	$\mathbf{\sigma}_0$	SPE	\mathbf{M}	\mathbf{m}_0	$\mathbf{\Sigma}$	$\mathbf{\sigma}_0$	SPE
(i)	50	.077	.074	.41	.43	.80	.110	.105	.41	.42	.48
	100	.057	.056	.29	.40	.51	.070	.066	.28	.34	.27
	200	.042	.043	.22	.34	.51	.048	.045	.19	.29	.41
	400	.027	.031	.14	.35	.61	.041	.040	.12	.27	.61
(ii)	50	.089	.080	.35	.28	.07	.102	.097	.43	.39	.05
	100	.065	.060	.27	.22	.05	.073	.070	.25	.23	.03
	200	.043	.041	.18	.17	.04	.048	.045	.19	.17	.02
	400	.032	.030	.13	.13	.03	.039	.037	.13	.12	.02
(iii)	50	.076	.068	.38	.27	.23	.110	.105	.38	.36	.18
	100	.054	.054	.29	.22	.21	.071	.067	.26	.23	.13
	200	.036	.042	.20	.18	.19	.053	.050	.18	.15	.09
	400	.027	.033	.15	.16	.17	.033	.031	.13	.11	.06

Table 1: Simulation Results. Relative root mean squared errors of parameter estimators.

Table 1. Biases and standard deviations can be found in the Supplementary Material.

We see in Table 1 that the mean and covariance estimators at the observed sites, $\hat{\mathbf{M}}$ and $\hat{\mathbf{\Sigma}}$, are consistent as n increases, and the magnitudes of the errors do not depend on the grid, as expected. The estimation errors of $\hat{\mathbf{m}}_0$ do not depend on the grid either because, for these models, the mean functions $\mu(t, \mathbf{s}_j)$ are nearly identical for all \mathbf{s}_j 's. However, the situation is different for the covariance estimator $\hat{\mathbf{\sigma}}_0$, since the true covariance function does change substantially with \mathbf{s} . The errors are larger for the sparser grid (i), and smaller for grids (ii) and (iii), being of comparable size for the last two. The behavior of $\hat{\mathbf{\sigma}}_0$, then, fundamentally depends on grid spacing, not grid size. The accuracy of the kriging predictor, on the other hand, is better under grid (ii) than under grid (iii), which shows that under comparable grid spacings, a smaller and more parsimonious grid is generally preferable. However, this behavior is model dependent: for Model 2, where $g(\mathbf{s})$ does not decrease away from \mathbf{s}_0 , spatial sites further away from \mathbf{s}_0 contribute more to prediction than under Model 1, so the error magnitudes under grids (ii) and (iii) are not as different for Model 2 as for Model 1.

Figure 1: Divvy data analysis. (a,b) Observed and (c,d) predicted daily count functions for (a,c) Union station and (b,d) Lasalle station.

5 Application: predicting bike demand

As an example of application, in this section we analyze data from the bicycle-sharing system of the city of Chicago, known as Divvy. The data is publicly available at the Chicago Data Portal website, <https://data.cityofchicago.org>. We will analyze bike trips that took place on laborable days of 2016, i.e. weekdays that were not holidays, in the downtown area known as ‘the Loop’, which is delimited by avenues Grand, Roosevelt and Halsted on the north, south and west, respectively, and the lake front on the east. There were 68 active stations in this area during this period. We specifically study bike check-out times, which can be modelled as replicated temporal Poisson processes; there are $n = 254$ replications in this sample, corresponding to the laborable days of 2016.

We will set aside two of the 68 bike stations for prediction: the one at the Union train station, on Adams and Canal Streets, and the one at Lasalle Avenue and Calhoun Street. These two stations exhibit two very different usage patterns: the

Union station shows a bimodal pattern with peaks at 8am and 5pm, the morning and evening work commutes, whereas the Lasalle station shows a unimodal pattern with peak at 5pm, the afternoon work commute. Their daily count functions are shown in Figure 1(a)-(b). Kriging prediction for these two stations will then be based on the other $d = 66$ stations in the Loop.

For estimation we used cubic B -splines with five equally-spaced knots as temporal basis $\beta(t)$ and tensor-product cubic B -splines with six equally-spaced knots on each coordinate as spatial basis $\gamma(\mathbf{s})$. The optimal smoothing parameters ξ_B and ξ_C were chosen by generalized cross-validation. Prediction accuracy can be assessed by comparing the observed count functions $N_i(t)$ with the predicted counts $\hat{N}_i(t)$. The root average squared error $\{\sum_{i=1}^n \|N_i - \hat{N}_i\|^2/n\}^{1/2}$, where $\|\cdot\|$ denotes the L^2 norm, is 184.2 for the Union station and 70.9 for the Lasalle station.

It is not surprising that the Union station is harder to predict. This bike station is situated at a train station and therefore has a peculiar pattern of demand, which is not shared by most other locations in the Loop. In contrast, the Lasalle station shows a more common pattern of demand. The average daily count for all the Loop stations is 56.9, similar to the average daily count of 52.7 for the Lasalle station, while the Union station has a much higher average daily count of 124.4. This sharp change in $\mu(t, \mathbf{s})$ at the Union station makes $\mu(t, \mathbf{s}_0)$ hard to estimate accurately.

The daily predicted counts are shown in Figure 1(c)-(d). The predictors capture the overall patterns of demand at both stations, but the morning commute peak is underestimated for the Union station. Figure 2 shows the best, median, and worst fits for each station. We see that the kriging predictor tends to underestimate the counts for the Union station and to overestimate them for the Lasalle station, but overall, prediction is accurate for the latter.

This example highlights both the possibilities and the limitations of spatial kriging for these types of problems. Prediction accuracy depends on the intrinsic variability at each station, which is independent of the other stations and therefore cannot be predicted, and on the degree of smoothness of the mean function $\mu(t, \mathbf{s})$ and the covariance functions $\Sigma(\mathbf{s}_j, \mathbf{s})$ at $\mathbf{s} = \mathbf{s}_0$. As long as the intrinsic variability is relatively low and there are no sharp peaks or troughs in $\mu(t, \mathbf{s})$ and $\Sigma(\mathbf{s}_j, \mathbf{s})$ at $\mathbf{s} = \mathbf{s}_0$, prediction will be accurate. But local landmarks like train stations, theaters, and stadiums, introduce spatial discontinuities that make prediction inaccurate when the estimators of $\mu(t, \mathbf{s}_0)$ and $\Sigma(\mathbf{s}_j, \mathbf{s}_0)$ are only based on spatial smoothing. Prediction

Figure 2: Divvy data analysis. (a,d) Best, (b,e) median and (c,f) worst fits for (a-c) Union station and (d-f) Lasalle station. (—) observed count function, (- - -) predicted count function.

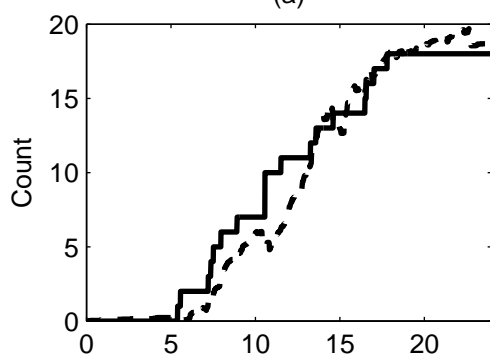
in these situations can likely be improved by introducing proximity to landmarks as covariates in the model, but this is a matter for further research.

References

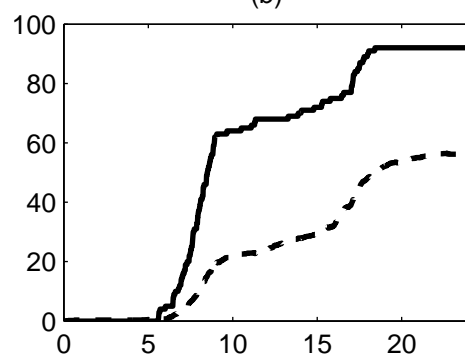
- Agarwal, G.G., and Studden, W.J. (1980). Asymptotic integrated mean square error using least squares and bias minimizing splines. *The Annals of Statistics* **8** 1307–1325.
- Buhmann, M.D. (2003). *Radial Basis Functions : Theory and Implementations*. Cambridge University Press, Cambridge, UK.
- Cressie, N. (1993). *Statistics for Spatial Data*. John Wiley & Sons, New York.
- De Boor, C. (2001). *A Practical Guide to Splines, Revised Edition*. Springer, New York.
- Gervini, D., and Khanal, M. (2019). Exploring patterns of demand in bike sharing

- systems via replicated point process models. *Journal of the Royal Statistical Society Series C: Applied Statistics* **68** 585–602.
- Giraldo, R., Delicado, P., and Mateu, J. (2010). Continuous time-varying kriging for spatial prediction of functional data: An environmental application. *Journal of Agricultural, Biological, and Environmental Statistics* **15** 66–82.
- Giraldo, R., Delicado, P., and Mateu, J. (2011). Ordinary kriging for function-valued spatial data. *Environmental and Ecological Statistics* **18** 411–426.
- Hastie, T., Tibshirani, R., and Friedman, J. (2009). *The Elements of Statistical Learning. Data Mining, Inference, and Prediction. Second Edition.* Springer, New York.
- Menafoglio, A., Secchi, P., and Dalla Rosa, M. (2013). A universal kriging predictor for spatially dependent functional data of a Hilbert space. *Electronic Journal of Statistics* **7** 2209–2240.
- Møller, J., and Waagepetersen, R.P. (2004). *Statistical Inference and Simulation for Spatial Point Processes.* Chapman and Hall/CRC, Boca Raton.
- Nair, R., and Miller-Hooks, E. (2011). Fleet management for vehicle sharing operations. *Transportation Science* **45** 524–540.
- Shaheen, S., Guzman, S., and Zhang, H. (2010). Bike sharing in Europe, the Americas and Asia: Past, present and future. *Transportation Research Record: Journal of the Transportation Research Board* **2143** 159–167.
- Stone, C. (1982). Optimal global rates of convergence for nonparametric regression. *The Annals of Statistics* **10** 1040–1053.
- Stone, C. (1994). The use of polynomial splines and their tensor products in multivariate function estimation. *The Annals of Statistics* **22** 118–184.
- Wahba, G. (1990). *Spline Models for Observational Data.* Society for Industrial and Applied Mathematics (SIAM), Philadelphia.
- Zhou, S., Shen, X., and Wolfe, D.A. (1998). Local asymptotics for regression splines and confidence region. *The Annals of Statistics* **26** 1760–1782.

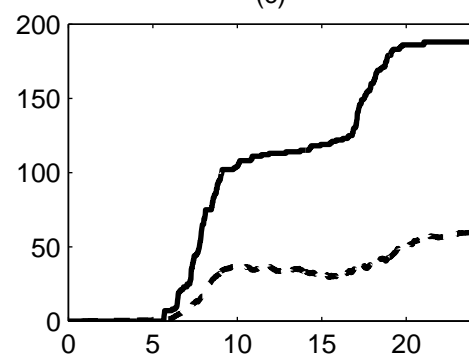
(a)



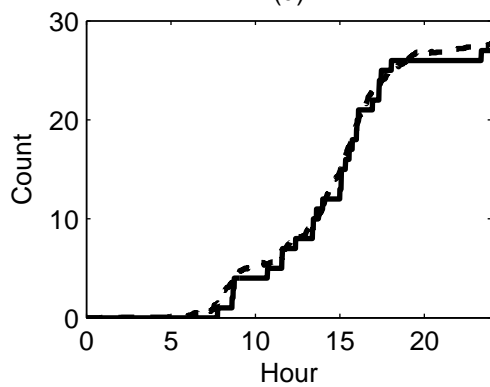
(b)



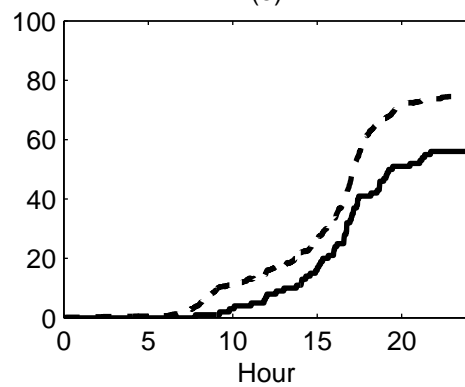
(c)



(d)



(e)



(f)

